

Article

An Inverse-Filter-Based Method to Locate Partial Discharge Sources in Power Transformers

Hamidreza Karami ^{1,2,*}, Farzane Askari ³ , Farhad Rachidi ¹ , Marcos Rubinstein ⁴  and Wojciech Sikorski ^{5,*} 

¹ Ecole Polytechnique Fédérale de Lausanne (EPFL), Electromagnetic Compatibility Laboratory, 1015 Lausanne, Switzerland; farhad.rachidi@epfl.ch

² Department of Electrical Engineering, Bu-Ali Sina University, Hamedan 6516738695, Iran

³ Department of Electrical Engineering, Technical and Vocational University (TVU), Tehran 1435661137, Iran; faskari@tvu.ac.ir

⁴ Institute for Information and Communication Technologies, University of Applied Sciences and Arts Western Switzerland (HES-SO), 1401 Yverdon-les-Bains, Switzerland; marcos.rubinstein@heig-vd.ch

⁵ Faculty of Electrical Engineering, Poznan University of Technology, 60-965 Poznan, Poland

* Correspondence: hamidreza.karami@epfl.ch (H.K.); wojciech.sikorski@put.poznan.pl (W.S.); Tel.: +41-21-693-48-18 (H.K.)

Abstract: Partial discharge (PD) occurrence in power transformers can lead to irreparable damage to the power network. In this paper, the inverse filter (IF) method to localize PDs in power transformers is proposed. To the best of the authors' knowledge, this is the first time that the inverse filter method has been used to localize PD sources in the electromagnetic regime. The method comprises two phases: the forward phase and the backward or backpropagation phase. In the forward phase, the waveform emitted from the PD source is recorded with one or several sensors. In the backward phase, the recorded signal is transformed into the frequency domain, inverted, transformed back into the time domain, and then back injected into the medium. Finally, a suitable criterion is used to localize the PD source. The efficiency of the proposed IF method is assessed considering different scenarios. It is shown that, for the considered configurations, the proposed IF method outperforms the classical time-reversal technique.

Keywords: partial discharge; inverse filter method; electromagnetic regime; source localization; power transformer; deconvolution method; time-reversal method



Citation: Karami, H.; Askari, F.; Rachidi, F.; Rubinstein, M.; Sikorski, W. An Inverse-Filter-Based Method to Locate Partial Discharge Sources in Power Transformers. *Energies* **2022**, *15*, 1988. <https://doi.org/10.3390/en15061988>

Academic Editor: Sérgio Cruz

Received: 27 January 2022

Accepted: 4 March 2022

Published: 9 March 2022

Publisher's Note: MDPI stays neutral with regard to jurisdictional claims in published maps and institutional affiliations.



Copyright: © 2022 by the authors. Licensee MDPI, Basel, Switzerland. This article is an open access article distributed under the terms and conditions of the Creative Commons Attribution (CC BY) license (<https://creativecommons.org/licenses/by/4.0/>).

1. Introduction

Diagnosing damage early in high-voltage equipment used in power systems has a vital role in the stability of the network. Failures in the equipment can lead to irreparable damage to the system. Partial discharge (PD) can occur in power transformers, gas-insulated substations (GIS), and power cable installations [1]. PDs cause erosion and failure in the equipment's insulation and reduce reliability in the network, imposing an extra cost for high-voltage installation owners. Therefore, monitoring partial discharge occurrence in equipment is important to prevent hazardous consequences [2,3].

A PD is a localized electric discharge that occurs within the insulation of the medium and has different measurable physical properties such as charge movement, acoustic emission, EM radiation, and chemical reaction. Based on these properties, PD signals can be detected by different techniques, including electrical, acoustic, ultra-high frequency (UHF) electromagnetic, optical, and chemical detection. Some of these techniques can diagnose PDs on-site and monitor in-service equipment [4,5].

PDs emit electromagnetic waves in the 300 MHz–3 GHz frequency range in the surrounding medium [6]. Based on the onset time or angle information of the UHF signals emitted by PDs, several electromagnetic methods have been developed, such as the time of arrival (ToA) [7], time difference of arrival (TDoA) [8,9], and angle of arrival (AoA) [10,11]

methods. Among them, TDoA is the most commonly used method to localize PDs inside power transformers. In [12–14], a 3D PD localization method has been proposed to locate PDs in power transformers based on TDoA. However, localization by TDoA is challenging because the onset time of the arrival of the signal is hard to determine with sufficient accuracy due to dispersion and noise. The TDoA method also needs at least four time-synchronized sensors to operate. Another problem with TDoA is that it requires a line of sight between the PD source and the sensors, a condition which is not always satisfied because of the presence of transformer windings.

More recently, time reversal (TR) in both the electromagnetic (EMTR) and the acoustic (ATR) regimes has been applied to locate PDs [15–18]. The TR technique can perform both 2D and 3D localization of multiple PD sources with only one sensor and does not require a line of sight. A typical TR process includes three steps: (1) recording the PD-emitted field by at least one sensor, (2) back injecting the time-reversed version of the measured signals into the medium using numerical simulations, and (3) using a suitable criterion to obtain the time and location at which the back-injected signals refocus. It should be noted that a degradation in the accuracy of the localization is observed when the PD is located near a metallic plane or object (within $\lambda_{min}/2$, where λ_{min} is the minimum wavelength) [17].

The inverse filter (IF) or deconvolution method is used as a technique to obtain the temporal compression of the focal signal [19]. It has been shown [20] that the IF method improves temporal and spatial focusing for both acoustic and elastic waves. It should be noted that the IF method can be used to reconstruct the source signal as well.

In [21,22], the IF method is applied in image processing for image restoration and reconstruction. It was shown in [23,24] that the IF method has tighter time-domain focusing and its sidelobes are substantially smaller than the TR method.

In this paper, we propose using an IF-based method to locate PDs, which consists of the following steps:

Step 1. The radiation from the (PD) source(s) is measured by a single sensor in the time domain.

Step 2. The received signal is transformed into the frequency domain using the fast Fourier transform (FFT). The obtained frequency-domain signal's spectrum is multiplicatively inverted and then back transformed into the time domain.

Step 3. The time-domain signal obtained in Step 2 is back injected numerically from the sensor into the simulation domain that contains the source.

Step 4. Finally, using a suitable criterion, the PD source is localized.

To the best of the authors' knowledge, the IF method has not been used in the electromagnetic regime. Furthermore, it has not been applied to locate PD sources. In this paper, we investigate for the first time the use of the IF method to localize PD sources in power transformers in the electromagnetic regime. In this paper, the proposed method will be named Electromagnetic Inverse Filter (EMIF) to distinguish it from the standard electromagnetic time-reversal method, known as EMTR. The performance of the EMIF method to localize the PD source will also be compared with that of the EMTR method.

The rest of the paper is organized as follows: In Section 2, we present the theory of the proposed method. Two-dimensional and 3D numerical simulations applying the proposed EMIF method to a power transformer are presented in Section 3, making reference to the classical EMTR method. The conclusions of the paper are presented in Section 4.

2. Electromagnetic Inverse Filter Theory

Two main phases are needed to implement the proposed EMIF method, the forward phase and the backward phase. To present the EMIF method, consider that there is one sensor inside the power transformer tank. A PD occurring inside the transformer tank emits an electromagnetic wave in the 300 MHz to 3 GHz frequency band which is recorded by the sensor.

The power transformer with the PD source and sensor can be considered a linear, time-invariant (LTI) system. Ignoring the noise, the signal received by the sensor $r(t)$ can thus be obtained as follows,

$$r(t) = s(t) * h(t) \quad (1)$$

where $s(t)$ is the PD source signal, $h(t)$ is the impulse response (or time-domain Green's function) that characterizes the propagation from the PD to the sensor, and $*$ is the convolutions operator. In this paper, the noise is ignored. The oscillations in the time-domain Green's function are the result of the multiple reflections from the transformer walls. Figure 1 shows an example of the convolution process.

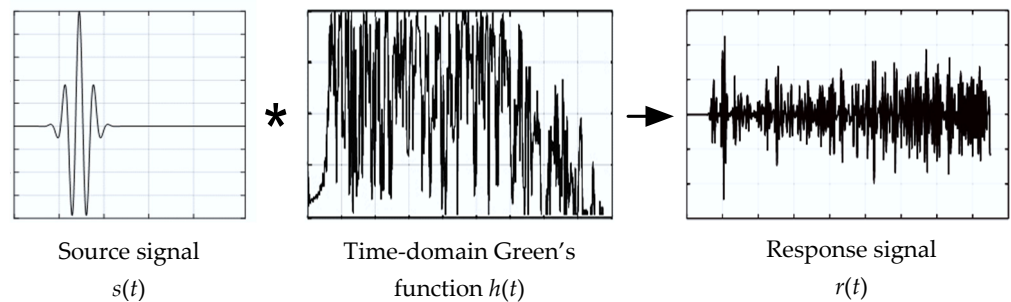


Figure 1. Received signal by the sensor due to a PD source signal considering the transformer as a linear, time-invariant system.

The time-domain Green's function $h(t)$ depends on the material and geometry of the power transformer and on the location of both the PD source and the sensor inside the tank.

Converting Equation (1) into the frequency domain, the convolution operator ($*$) is replaced by multiplication as follows,

$$R(\omega) = S(\omega)H(\omega) \quad (2)$$

where ω is the angular frequency, and capital letters are used to represent the frequency-domain transforms of the time-domain quantities [22].

The forward phase of the EMIF method process involves recording the signal $R(\omega)$ at the sensor location due to a PD source signal. This can be done either directly in the frequency domain or by measuring $r(t)$ and using the Fourier Transform.

In the backward phase, the frequency-domain signal at the sensor location, $R(\omega)$, is inverted and back injected into the medium from the sensor's location. The back injection is performed by simulation.

After back injecting the inverted signal, the whole computation domain is probed using virtual (or test) sensors. Two cases can be considered in the backward phase. The first case is when the test sensor is located at the actual PD source location. The second case is when the test sensor is located at locations other than the actual PD source location.

In the first case, due to the reciprocity theorem, the transfer function of the backward phase is identical to that of the forward phase. The signal received at a test point located at the actual PD source, $Y(\omega)$, is obtained by multiplying the inverted signal by the transfer function $H(\omega)$,

$$Y(\omega) = \frac{1}{S(\omega)H(\omega)}H(\omega) = \frac{1}{S(\omega)} \quad (3)$$

It can be seen in Equation (3) that the back-propagated signal at the PD source location is equal to the inverted frequency-domain PD source signal.

In the second case, since the test point is located at an arbitrary point except for the actual PD source location, the transfer function of the backward phase $G(\omega)$ is different

from that in the forward phase $H(\omega)$. This means that the received signal $Y(\omega)$ at the test point is given by

$$Y(\omega) = \frac{1}{\overline{S(\omega)H(\omega)}}G(\omega) = \frac{1}{\overline{S(\omega)}}\frac{G(\omega)}{H(\omega)} \quad (4)$$

According to Equation (4), the received signal at points other than the actual PD source location is different from the inverted function of the frequency-domain PD source signal.

Since the PD source signal is a short-duration signal, we assume here, as an example (we will use another waveform later on in the simulations), that the PD source signal is a Dirac delta function $\delta(t)$. Therefore, when the test point coincides with the actual PD source location, the received signal is a Dirac delta function $\delta(t)$ as well. At other test points, according to Equation (5), when the PD source is a Dirac delta function $\delta(t)$, the received time-domain signal at the test point is given by

$$y(t) = IFT\left\{\frac{G(\omega)}{H(\omega)}\right\} \quad (5)$$

where IFT is the inverse Fourier transform [20]. It can be seen that the width of the reconstructed signal at any test point except the actual PD location is nonzero.

Note also that Equation (3) can be rewritten as:

$$Y(\omega) = \frac{1}{S(\omega)} = \frac{\overline{S(\omega)}}{|S(\omega)|^2} \quad (6)$$

where $\overline{}$ is the conjugate operator, which corresponds to the time-reversal operation in the time domain. This shows inverse filtering can actually be considered as a time-reversal technique with magnitude compensation in the frequency domain [24].

Avoiding Division by Zero in the Inverted Frequency-Domain Signal

Inverting frequency-domain quantities requires special care when they take zero or close to zero values. To cope with this problem, the inverted frequency-domain signal used in the backward phase can be mathematically manipulated as follows:

$$\frac{1}{\overline{S(\omega)H(\omega)}} = \frac{1}{S(\omega)H(\omega)}\frac{\overline{S(\omega)H(\omega)}}{\overline{S(\omega)H(\omega)}} = \frac{\overline{S(\omega)}\overline{H(\omega)}}{|S(\omega)H(\omega)|^2} \quad (7)$$

where, again, $\overline{}$ is the conjugate operator and $||$ is the absolute operator. If $S(\omega)H(\omega) = 0$ at a given frequency, the denominator of Equation (7) becomes zero. To avoid division by zero in the EMIF method in calculating Equation (7), a constant term, ε , dependent on the mean value of the received signal in the frequency domain is added to the denominator.

$$\frac{\overline{S(\omega)}\overline{H(\omega)}}{|S(\omega)H(\omega)|^2 + \varepsilon} \quad (8)$$

where

$$\varepsilon = \alpha \text{mean}\left(|S(\omega)H(\omega)|^2\right) \quad (9)$$

In (9), α is a constant chosen to optimally reduce the effect of noise introduced through the inverse filtering procedure. It has been set to 0.9 as suggested by Douma and Neiderleithinger in [24].

Equation (8) is used to invert the frequency-domain signal in the backward phase. After that, the time-domain waveform of the inverted signal is obtained and back injected into the medium. According to Equation (3), the reconstructed signal should have a high spatiotemporal concentration at the location of the actual PD source.

3. Numerical Simulations and Results

This section aims at evaluating the performance of the EMIF method to localize PD sources in power transformers. The section is divided into three subsections. In Section 3.1, a simple 2D model is used to represent the transformer tank. The windings inside the transformer tank are modeled using metallic cylinders. Using a 2D model leads to a reduced computation time for the forward and backward phases needed in the proposed EMIF method. In Section 3.2, the performance of the EMIF method is evaluated using a simple 3D model for the transformer. The assumed model is simulated using the commercial software CST-MWS. In both subsections, comparisons between the proposed method and classical EMTR are also provided. Finally, in Section 3.3, a laboratory transformer model implemented in the CST-MWS software is used to assess the performance of the proposed method to localize a PD source inside a realistic power transformer tank.

3.1. 2D Transformer Model

Figure 2 shows the adopted 2D model to simulate a three-phase transformer. The transformer tank is modeled by a rectangular shape. Its length and width, l and w , are equal to 1000 mm and 500 mm, respectively. The material of the transformer walls is considered to be a perfect electric conductor. The three solid cylindrical windings inside the transformer are modeled as three metallic $a/2 = 100$ mm radius circles. The circular barriers in Figure 2 represent the outer radius of the three-phase transformer windings. The center of the middle winding coincides with the center of the tank. The edge-to-edge distance between two adjacent windings is $b = 50$ mm. The considered model for the 2D transformer is symmetric about the x and the y axes. The transformer tank is considered to be empty. In other words, no insulating equipment (such as paper pressboard) or magnetic circuit (core) is considered in the transformer tank. Note that, even though the model used here is a simplified transformer model, it has been shown that the performance of the time-reversal method is improved in more complex and heterogeneous media due to the effect of multiple reflections [25].

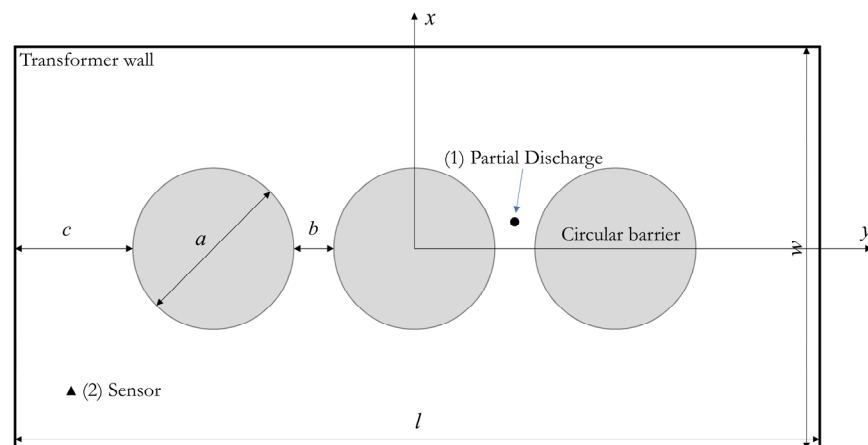
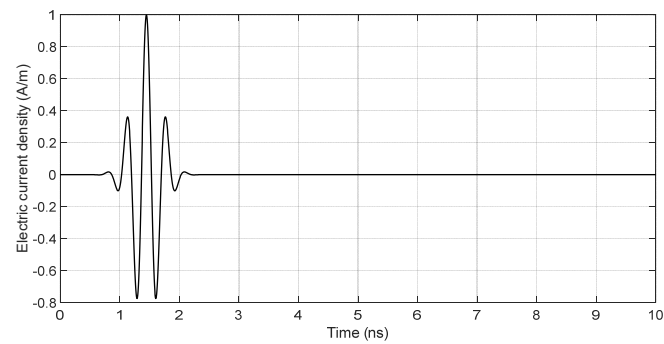
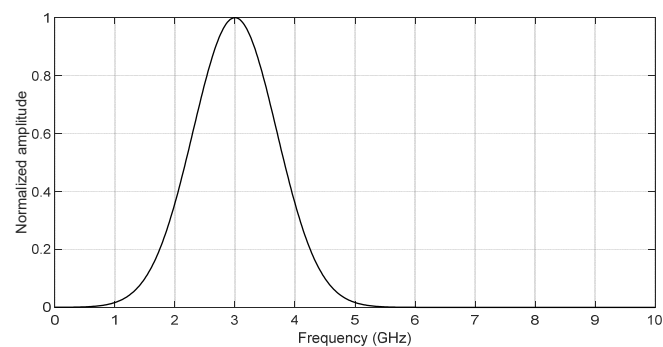


Figure 2. The geometry of the 2D transformer model.

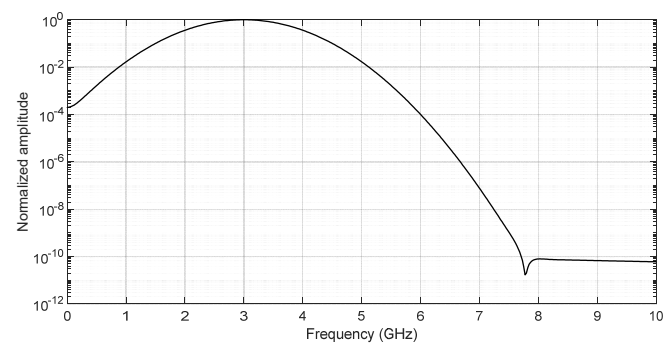
In Figure 2, the locations of the PD source (point #1) and sensor (point #2) are denoted by a black circle and a triangle, respectively. The shown locations of the PD source and sensor in Figure 2 are arbitrary and they are shown only for illustration purposes. In all the 2D simulations, one sensor and one PD source are considered. To implement the proposed EMIF method, a cosine-modulated Gaussian pulse is considered for the PD source signal, as shown in Figure 3a. The magnitude of the frequency-domain transform of this cosine-modulated Gaussian pulse is shown in Figure 3b,c in linear and logarithmic scale, respectively. The center frequency and bandwidth for the signal in Figure 3 are 3 GHz and 3 GHz, respectively. Depending on the case study, different values for the bandwidth and frequency center are used in this paper.



(a)



(b)



(c)

Figure 3. The cosine-modulated Gaussian pulse used as the PD source: (a) time-domain waveform; (b) magnitude spectrum in linear scale; (c) magnitude spectrum in logarithmic scale.

For the 2D simulations, five case studies (CS#1 to CS#5) are considered with different locations of the source and the sensor (see Table 1). In the first and second case studies, the windings (see Figure 2) are not included in the model.

Table 1. The list of case studies in the 2D simulations.

Case Studies	Windings Incl. (Y/N)	Sensor Location (x,y) m	Source Location (x,y) m	Center Frequency, Bandwidth (GHz)
CS#1	N	(−0.25, 0.2)	(0.25, −0.2)	3, 3
CS#2	N	(−0.35, −0.2)	(0.3, 0.24)	3, 3
CS#3	Y	(−0.25, −0.2)	(0.125, 0.0)	3, 3
CS#4	Y	(−0.25, 0.2)	(0.25, −0.125)	1.5, 1.5
CS#5	Y	(−0.25, 0.2)	(0.125, 0.0)	2.0, 1.5

The 2D finite-difference time-domain (FDTD) technique was used to solve Maxwell's equations in the transverse magnetic mode. In other words, one electric field component (E_z) and two magnetic field intensity components (H_x and H_y) will be used to solve Maxwell's equations. In the FDTD technique, equally spaced mesh cells along the x and y axes are considered with a length of 2.5 mm. The time step used in the simulations, rounded to one decimal place, is 5.3 picoseconds. It should be noted that the sensor is modeled using a single-point field probe that records the electric field calculated by the FDTD method.

3.1.1. CS#1: Transformer Tank Model without Windings

In this case study, the source and sensor locations are respectively at positions (0.25 m, -0.2 m) and (-0.25 m, 0.2 m). The excitation signal for the source is shown in Figure 3. The number of iterations in the FDTD simulation is 8192 time steps (corresponding to a time window of 43 ns).

Figure 4a,b show the time- and normalized frequency-domain waveforms of the electric field intensity recorded by the sensor. The resonance shown in Figure 4a is due to the multiple reflections from the walls of the transformer tank. To apply the proposed EMIF method, the inverted version of the signal received by the sensor in the frequency domain is calculated using Equation (8) with $\alpha = 0.9$. The normalized inverted frequency-domain signal received by the sensor is shown in Figure 4c. This inverted signal is transformed to the time domain using the inverse fast Fourier transform and then back injected into the transformer tank model.

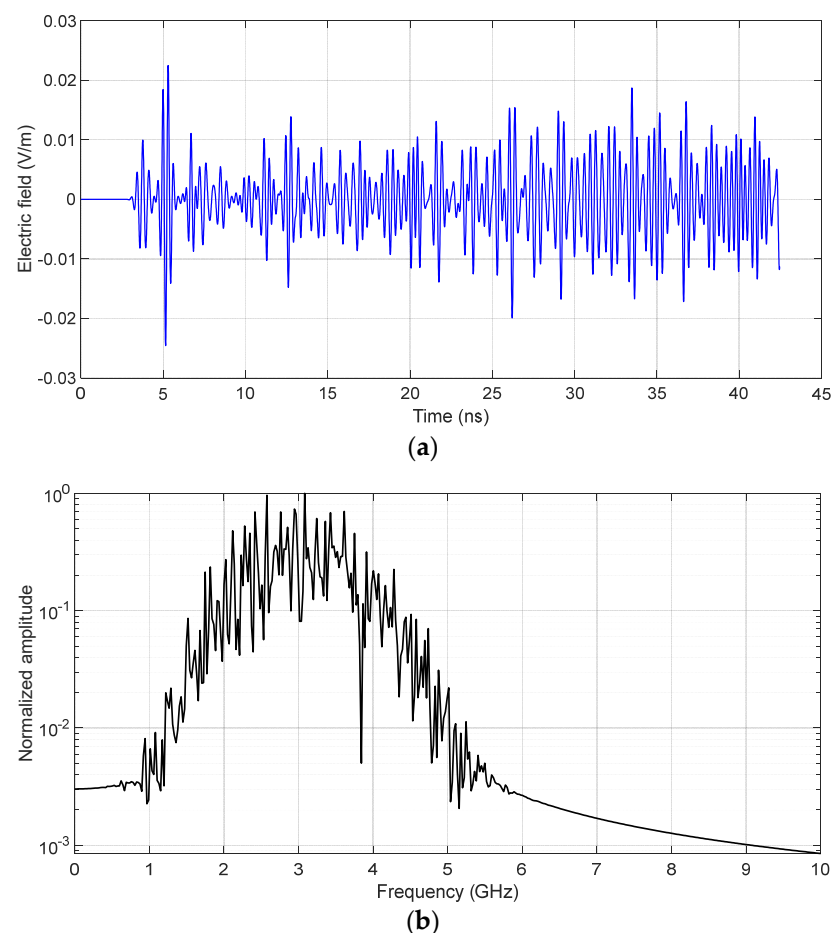


Figure 4. Cont.

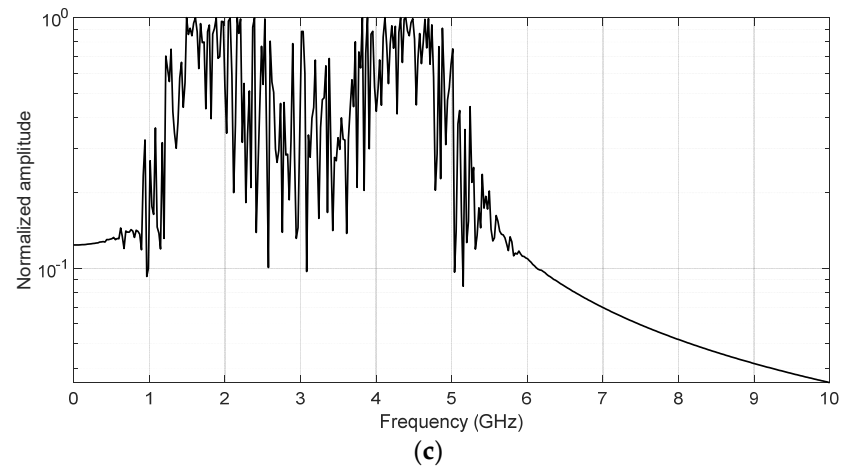


Figure 4. (a) The time-domain signal received by the sensor; (b) the normalized frequency-domain signal (magnitude) received by the sensor (logarithmic scale); (c) the normalized inverted signal (magnitude) received by the sensor in the frequency domain (logarithmic scale).

After doing the backward simulation using the FDTD method with the same parameters as in the forward phase, the distribution of the normalized maximum electric field power over the whole time interval is shown in Figure 5a. In all the figures, the colors represent the intensity of the represented quantity. In that figure, the red circle (o) and black cross (×) show the actual and estimated source locations, respectively. The location of the sensor is shown by the pink square (□) in Figure 5a. An expanded view of the region close to the source location is shown in the figure inset. The localization error for the proposed EMIF method is zero. In Figure 5, to estimate the location of the source, the maximum power criterion proposed in [18] is used. The length of the square mask window around the sensor (used to exclude the sensor from the maximum power search domain) is 25 cells along the x - and y -axes.

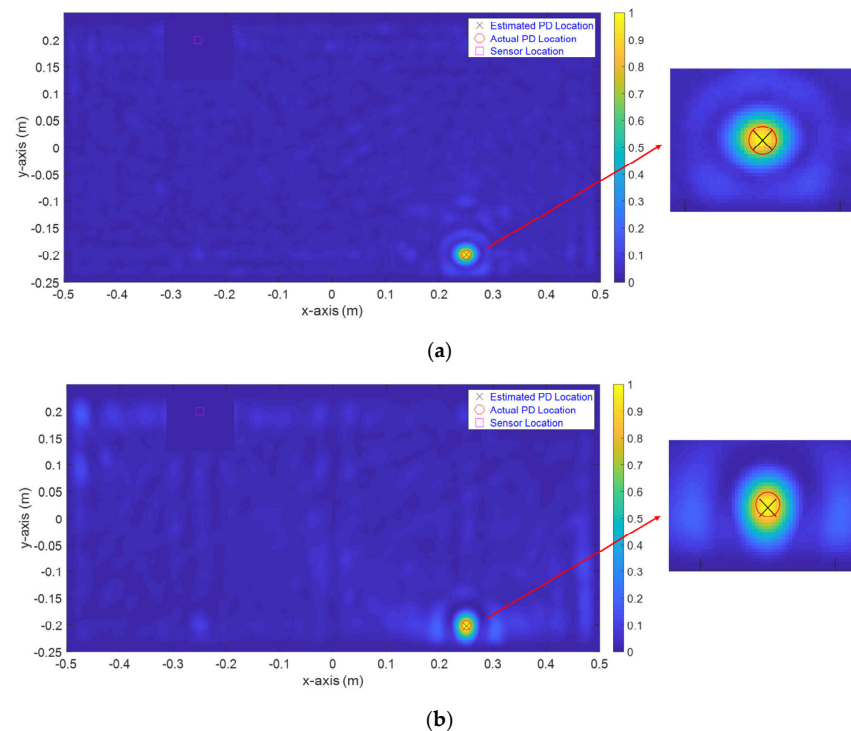


Figure 5. The distribution of the normalized maximum electric field power over the whole time interval in the computational domain, (a) obtained by the EMIF method and (b) obtained by the EMTR method. The localization errors are 0 for EMIF and 25 mm for EMTR.

For the sake of comparison, the distribution of the normalized maximum electric field power over the computational domain obtained using the classical EMTR method is shown in Figure 5b. An expanded view for the source region is also shown in the figure inset. The red circle (o) and the black cross (\times) show the actual and estimated source locations, respectively. The localization error with the EMTR method is 2.5 mm, namely, equal to a mesh cell.

It can be seen that both the EMIF and the EMTR methods can easily localize the source inside the transformer tank with only one sensor. The accuracy of the EMIF method appears to be better than that of the EMTR method for this specific case.

3.1.2. CS#2: Localization of a PD Source Close to a Metallic Wall

In the second case study, CS#2, the performance of the EMIF method is compared to the EMTR method when the PD is located in the immediate vicinity of the metallic transformer wall. In this case, the source is located at point (0.3 m, 0.24 m), 10 cm away from the metallic wall, while the sensor is located at (−0.35 m, −0.2 m). The other parameters are the same as in CS#1.

Figure 6a,b show the distribution of the normalized maximum electric field power over the computational domain obtained by using the EMIF and the EMTR methods. In this figure, the red circle (o) and the black cross (\times) show the actual and estimated source locations, respectively. The location of the sensor is denoted by the pink square (\square). The length of the square mask windows used in the EMIF and EMTR methods is 20 cells [18]. An expanded view of the region around the source is shown in the insets to highlight the performance of both methods. The localization errors are, respectively, 10.3 mm and 17.5 mm for the proposed EMIF method and the classical EMTR method. This shows that EMIF performs better than EMTR in locating sources close to metallic walls.

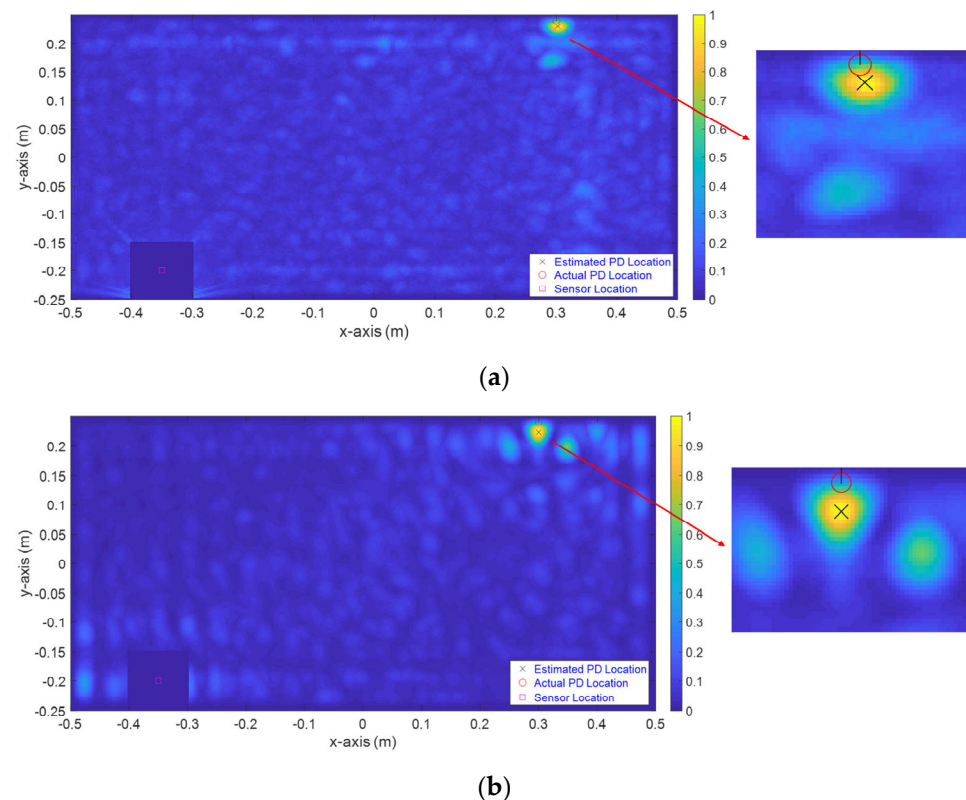


Figure 6. The distribution of normalized maximum electric field power over the complete simulation time interval on the computational domain, (a) obtained by the EMIF method with a 10.3 mm localization error and (b) obtained by the EMTR method with a 17.5 mm localization error.

3.1.3. CS#3: Localization of a PD Source between Two Metallic Windings

In the third case study, CS#3, three circular barriers representing the transformer windings are included in the transformer model. The windings are considered perfect electric conductor circles. The considered source is located between two windings. The coordinates of the PD source and the sensor are (0.125 m, 0.0 m) and (−0.25 m, −0.2 m), respectively. All the other parameters of the FDTD simulations are the same as in the first case study, CS#1.

The distributions of the normalized maximum electric field power over the computational domain obtained by the EMIF and EMTR methods are shown in Figure 7a,b, respectively. In this figure, the location of the sensor is denoted by the pink square (□). The red circle (o) and the black cross (×) show the actual and estimated source locations. An expanded view of the region around the source is shown in the EMIF figure inset.

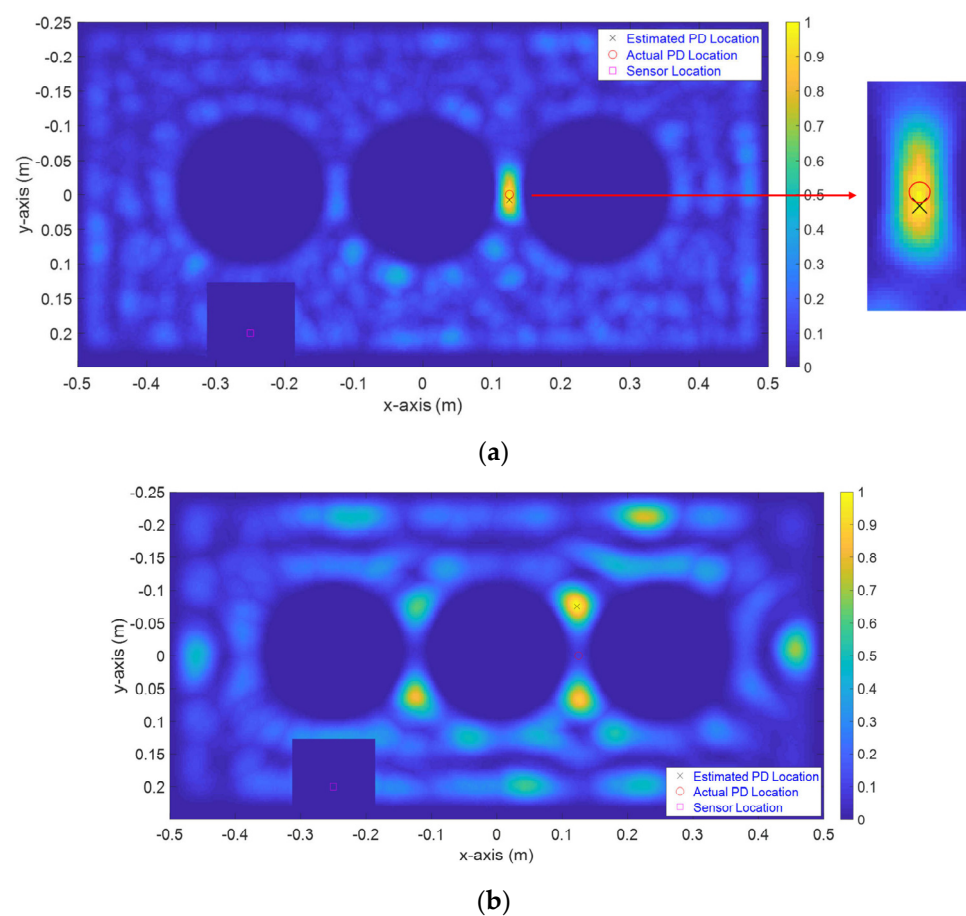


Figure 7. The distribution of normalized maximum electric field power over the complete simulation time interval on the computational domain, (a) obtained by the EMIF method with a 2.5 mm localization error and (b) obtained by the EMTR method with a 75.0 mm localization error. In this case study, the EMTR method cannot localize the source between two adjacent metallic objects.

The localization errors are 2.5 mm and 75.0 mm for the proposed EMIF method and EMTR, respectively. The length of the square mask windows used in both the EMIF and EMTR methods is 20 cells [18]. This case study shows that the proposed EMIF method is able to solve one of the main problems to localize sources located between the two adjacent metallic objects [17]. In this case study, the EMIF method shows a better performance compared to the classical EMTR method again.

3.1.4. CS#4: Localization of PD Source behind the Metallic Windings

In this case study, in addition to the presence of circle barriers or windings in the transformer tank, the PD source is behind the farthest metallic winding from the sensor. Note that, in this case study, compared to CS#3, no direct line of sight exists between the sensor and the PD source. In other words, the source of PD is hidden from the view of the sensor. The PD location coordinates are (0.25 m, -0.125 m), and the sensor is located at the point (-0.25 m, 0.2 m). The PD source signal in this case study is assumed to be a cosine-modulated Gaussian pulse with a bandwidth and a frequency center of 1.5 GHz. Due to the reduction in bandwidth in this example and to the location of the PD source behind the transformer winding, the localization is more challenging compared to the previous cases.

The number of iterations for CS#4 is 16,384 time steps, corresponding to around 87 ns. All the other parameters are the same as CS#1.

Figure 8a,b show the simulation results obtained by the EMIF method and the EMTR method, respectively. In this figure, the location of the sensor is denoted by the pink square (\square). The red circle (\circ) and the black cross (\times) show the actual and estimated source locations. An expanded view of the region around the source for the EMIF method is shown in the figure inset.

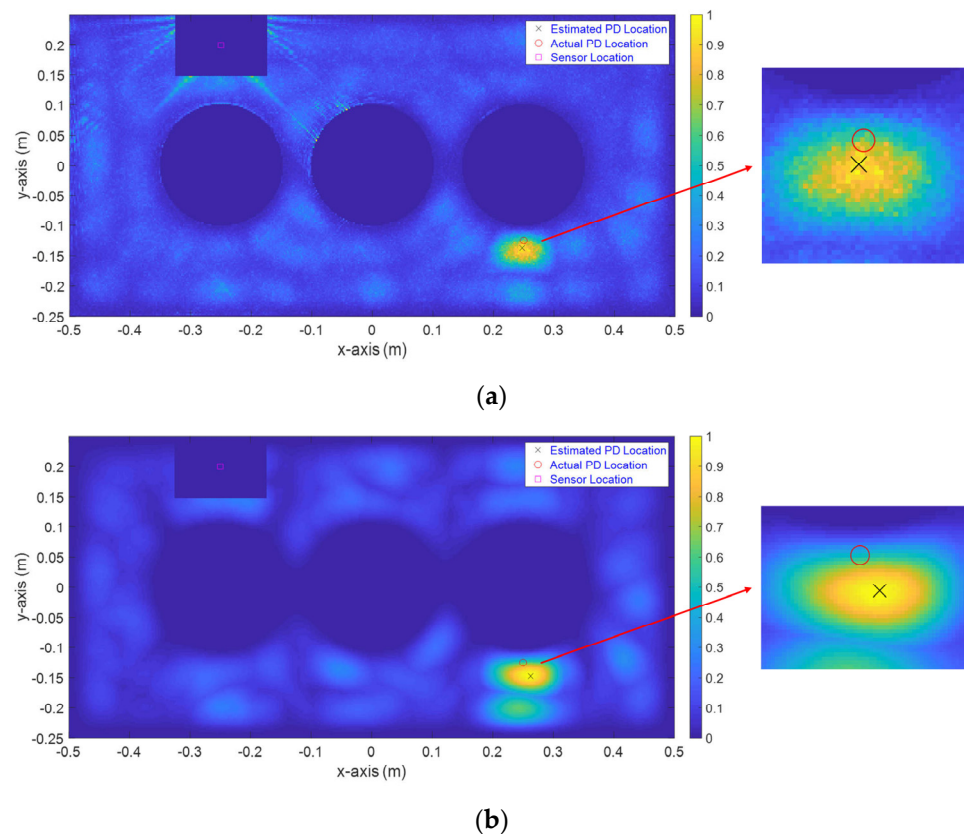


Figure 8. The distribution of normalized maximum electric field power over the complete simulation time interval on the computational domain, (a) obtained by the EMIF method with a 12.7 mm localization error and (b) obtained by the EMTR method with a 25.7 mm localization error.

The localization errors for the proposed EMIF method and EMTR are 12.7 mm and 25.7 mm, respectively. Again, the EMIF method shows a better performance compared to the classical EMTR method. The lengths of the square mask windows used in both the EMIF and EMTR methods are 30 and 20 cells along the x- and y-axes, respectively [18].

3.1.5. CS#5: Localization of a PD Source between the Metallic Windings

In the fifth case study, the location of the PD source and the sensor are (0.125 m, 0.0 m) and (−0.25 m, 0.2 m), respectively. The considered center frequency and bandwidth of the PD source waveform are 2.0 GHz and 1.5 GHz, respectively. All the other parameters are the same as in CS#4. Compared to CS#3, the center frequency and bandwidth of the excitation signal are reduced in this case study.

Figure 9a,b show the simulation results obtained by the EMIF and EMTR methods. In this figure, the location of the sensor is denoted by the pink square (□). The red circle (o) and the black cross (×) show the actual and estimated source locations. An expanded view of the region around the source for the EMIF method is shown in the figure inset.

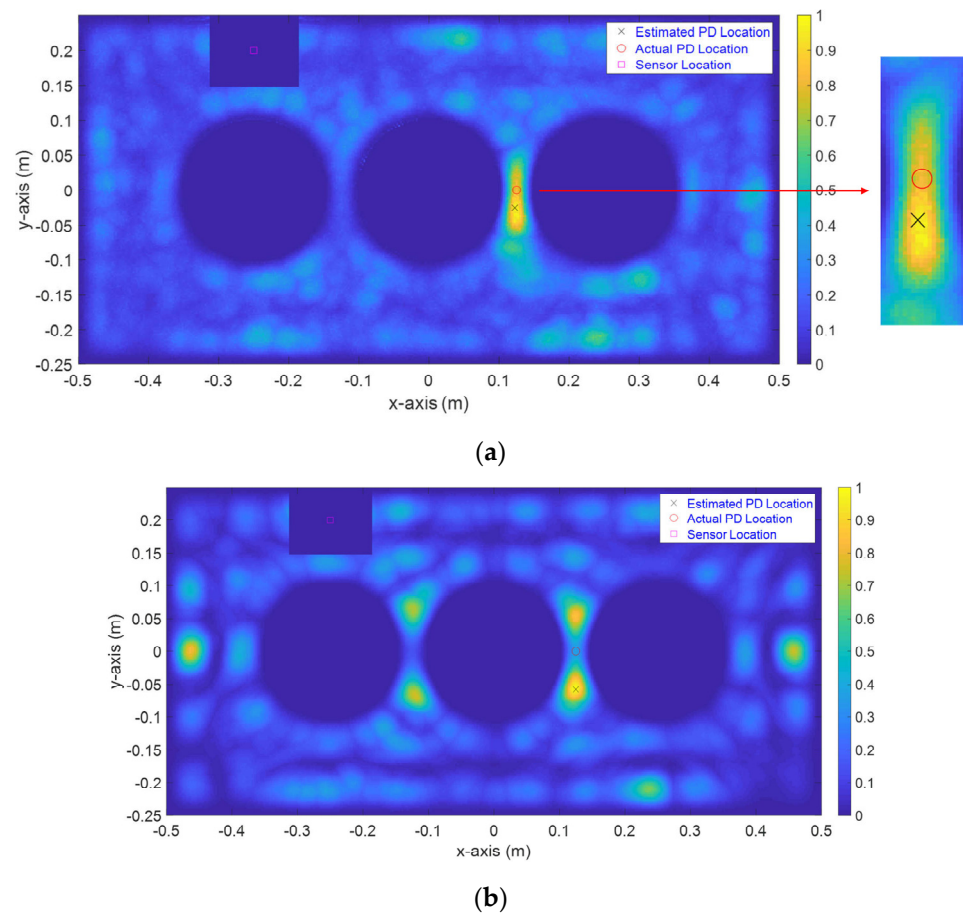


Figure 9. The distribution of normalized maximum electric field power over the complete simulation time interval on the computational domain, (a) obtained by the EMIF method with a 25.1 mm localization error, (b) obtained by the EMTR method with a 57.5 mm localization error. In this case study, the EMTR method cannot localize the source between two adjacent metallic objects.

The localization errors are 25.1 mm and 57.5 mm for the proposed EMIF method and for EMTR, respectively. Again, the EMIF method outperforms the classical EMTR method. The lengths of the square mask windows used in the EMIF and the EMTR methods are 30 and 20 cells along the x- and y- axes, respectively [18].

The degradation in the accuracy of the EMTR localization when the PD is located near a metallic plane or object (within $\lambda_{min}/2$, where λ_{min} is the minimum wavelength of the source) has been discussed in [17]. For the same reason, the EMIF location accuracy is also reduced but not as much as in the EMTR method, as indicated by the results associated with case studies CS#2, CS#3, and CS#5. This is essentially because the upper 3 dB cutoff frequency used for the EMIF method is higher than for the EMTR method (more energy in the higher frequencies), making $\lambda_{min}/2$ smaller.

In all the case studies, the obtained localization error by the EMIF method is significantly lower than that obtained using the EMTR method. The values of the localization error by both methods are summarized in Table 2.

Table 2. Localization errors by the EMIF and the EMTR methods in all 2D simulation case studies.

Case Studies	Localization Error (mm) by:	
	EMIF Method	EMTR Method
CS#1	0	25
CS#2	10.3	17.5
CS#3	2.5	75
CS#4	12.7	25.7
CS#5	25.1	57.5

3.2. A Simple 3D Transformer Model

In this section, a simple 3D model for the transformer tank is considered as shown in Figure 10. The size of the considered 3D tank is $1000 \times 500 \times 500 \text{ mm}^3$ in the direction of the x-axis, the y-axis, and the z-axis, respectively. The tank walls are assumed to be perfect electric conductors. Here, the 3D simulation commercial software CST-MWS is used to implement both the forward and backward simulations in the EMIF and EMTR methods. CST-MWS uses the finite integration technique (FIT) to solve Maxwell's equations in the time domain.

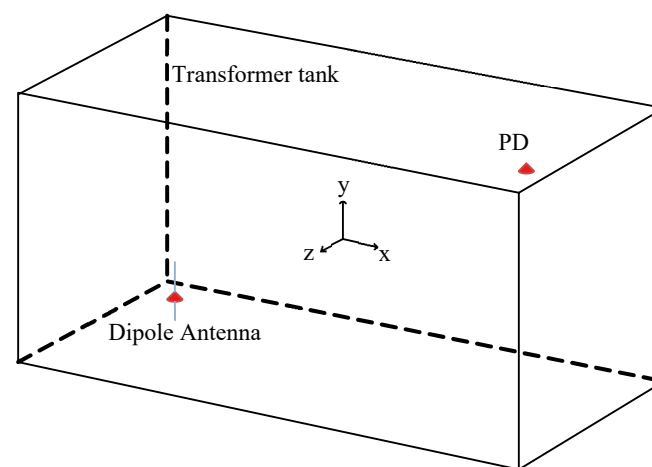


Figure 10. The geometry of the 3D transformer tank for simulation.

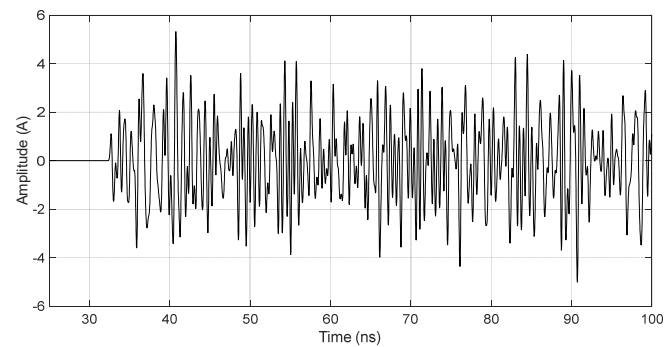
To model the sensor, a dipole antenna with a center frequency of 1 GHz is considered. The length, diameter, and gap parameter for this dipole antenna are 135 mm, 5 mm, and 20 mm, respectively. As shown in Figure 10, the direction of the dipole antenna is along the z-axis. A 72-Ohm resistance is used at the input of the dipole antenna. The center of the dipole antenna is placed at point $(-0.25 \text{ m}, -0.1 \text{ m}, 0.15 \text{ m})$ inside the transformer tank.

To model the PD source, a discrete port is modeled inside the transformer tank. The center of the PD source is $(0.3 \text{ m}, 0.16 \text{ m}, -0.1 \text{ m})$. A Gaussian pulse with a bandwidth of 3 GHz and 30 ns delay with respect to the one shown in Figure 3a is used to excite the PD source. The minimum and maximum frequencies in the CST-MWS are 0 and 3 GHz, respectively. The length and direction of the PD source are 20 mm and along the z-axis, respectively.

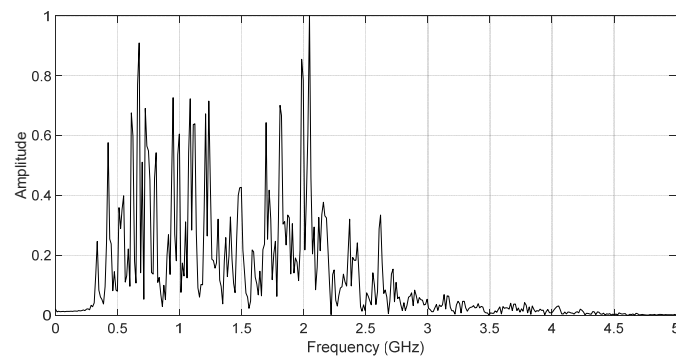
In the backward phase for both EMIF and EMTR, the electric field intensities over three orthogonal planes containing the PD source are monitored. To localize the PD source, the maximum field power criterion [18] is used over these three planes. In the backward

phase, the PD source is removed from the simulation model. The number of mesh cells and the time step used in the CST-MWS software are 1,292,000 and 4.89 ps, respectively.

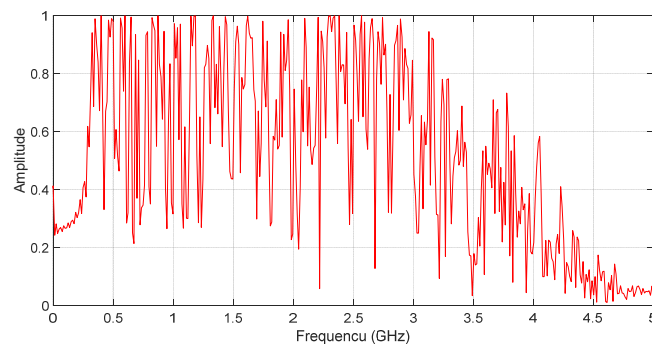
To implement the EMIF method, the simulation in CST-MWS is done for the forward phase. The recorded signal at the output of the dipole antenna is exported from CST-MWS and transformed to the frequency domain. Figure 11a,b show the time-domain waveform recorded by the dipole antenna and its normalized frequency-domain magnitude spectrum. The reason for the time fluctuations in the time-domain signal is the multiple reflections from the metallic walls of the transformer tank.



(a)



(b)



(c)

Figure 11. The signal received by the sensor installed in the 3D transformer tank modeled in the CST-MWS software: (a) time-domain waveform; (b) normalized magnitude spectrum of the time-domain waveform; (c) normalized magnitude spectrum of the inverted signal.

The signal received by the dipole antenna is inverted according to Equation (8) and transformed back into the time domain. The normalized magnitude spectrum of the inverted signal is shown in Figure 12c. Finally, in the backward phase, the time-domain

version of the inverted signal is back injected into the CST-MWS model of the transformer without the discrete port used to model the PD source.

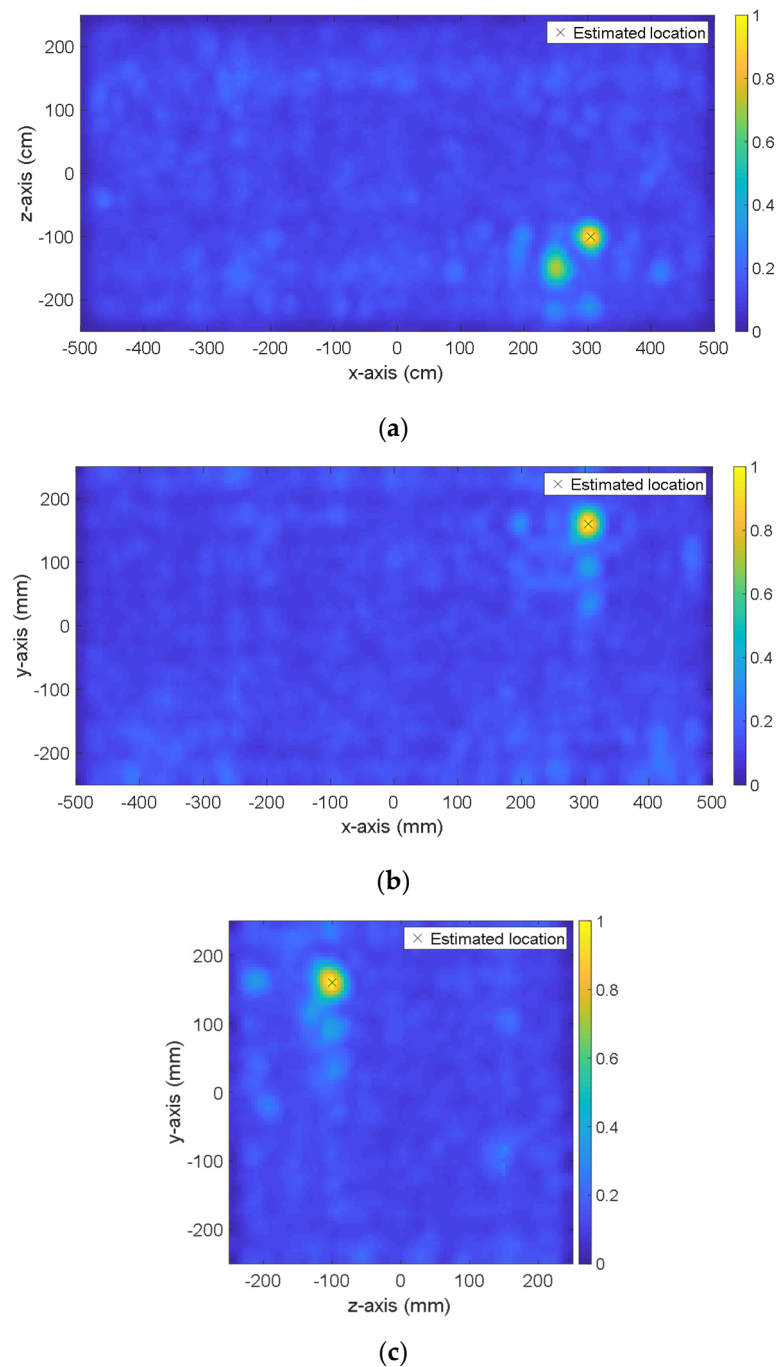


Figure 12. The distribution of normalized maximum electric field power over the complete simulation time interval in the computational domain for (a) cut-plane $y = 0.16$ m, (b) cut-plane $z = -0.10$ m, and (c) cut-plane $x = 0.3$ m. The black crosses (×) show the estimated location for the PD source. The localization error of the proposed EMIF method is 5 mm. In Equation (8), the parameter α used in the EMIF method is 0.9.

Figure 12a–c show the distribution of the normalized maximum electric field power over the computational domain obtained by the EMIF method in the three orthogonal cut-planes. In these figures, the estimated PD location is shown by the black cross (×).

If the center of the discrete port is considered as the actual location of the PD source, the 3D localization error in the EMIF method is 5 mm. The 3D localization error is defined as the 3D distance between the center of the discrete port used for the PD source and the estimated location obtained by the maximum field criterion. As in the 2D case studies presented earlier, here we use 0.9 as the value of the parameter α in the EMIF method.

Figure 13a–c show the distribution of the normalized maximum electric field power over the computational domain in three orthogonal cut-planes, obtained by the classical EMTR method. In these figures, the estimated PD location is shown by the black cross (\times).

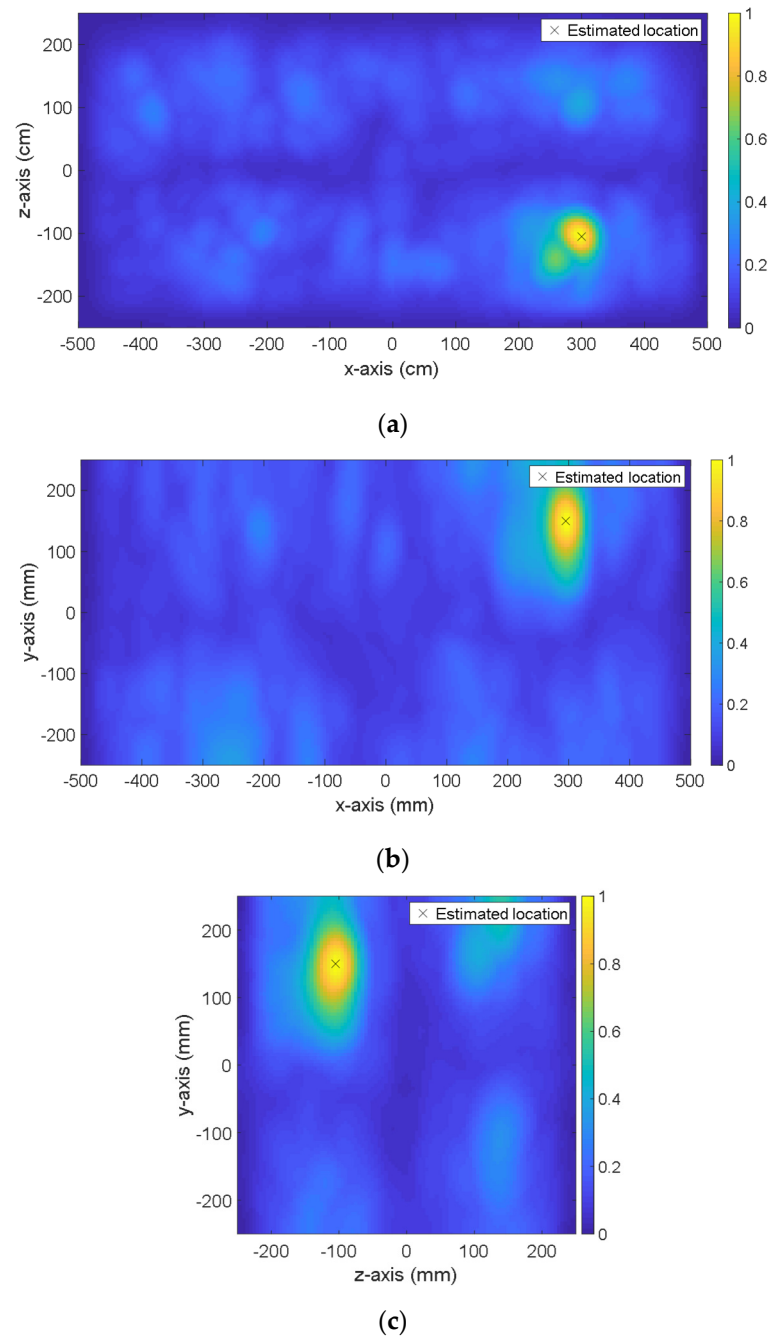


Figure 13. The distribution of normalized maximum electric field power over the complete simulation time interval in the computational domain for (a) cut-plane $y = 0.16$ m, (b) cut-plane $z = -0.10$ m, and (c) cut-plane $x = 0.3$ m. The black crosses (\times) show the estimated location for the PD source. The localization error of the classical EMTR method is 15.1 mm.

The 3D localization error in the EMTR method is about 15.1 mm. As for the 2D simulations, EMIF appears to be more accurate than EMTR in locating PD sources in 3D.

It is obvious from Figure 11b that the received signal has no significant frequency content beyond 3 GHz. On the other hand, as can be seen from Figure 11c, the inverted signal in the frequency domain has significant frequency content up to 4.5 GHz. This increase in the frequency bandwidth is one of the main reasons explaining why EMIF outperforms EMTR.

A comment is in order on the choice of the parameter α in Equation (8). So far, a value $\alpha = 0.9$ was adopted in the EMIF method simulations. This choice was based on reference [24], in which by changing the value of α , the temporal focus is calculated and it is shown that, by setting $\alpha = 0.9$, the maximum temporal focusing can be achieved. To evaluate the effect of the parameter α on the performance of the EMIF method, the last 3D case studies are repeated for the EMIF method for different values of α . In these simulations, the parameter α is varied from 0.1 to 100.

Figure 14 shows the distribution of the normalized maximum electric field power over the whole time interval in the computational domain for different values of α from 0.1 to 100 in the EMIF method (see Equation (8)). It can be seen that the variation of α can affect the focal spot and the localization error in the EMIF.

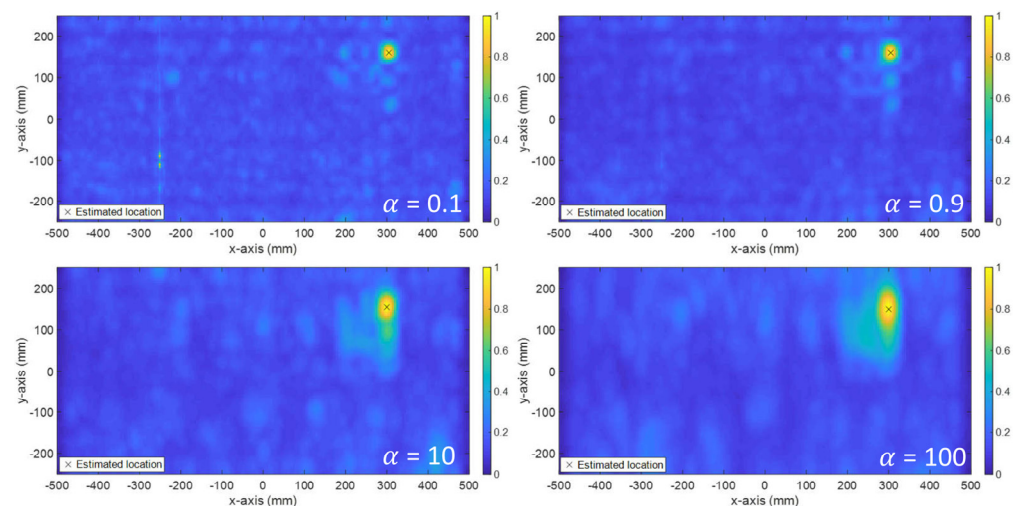


Figure 14. The distribution of the normalized maximum electric field power over the complete simulation time interval in the computational domain for different values of α .

By increasing the parameter α , both the focal spot sharpness and the accuracy are degraded. Based on the authors' experience and multiple simulations (not included in this paper), the range for α that yields the best EMIF results is (0.1–5). It should be noted that more investigation is needed to determine this range for other applications.

3.3. A More Realistic 3D Transformer Model

In the last case study, a more realistic transformer model is adopted. The model consists of a transformer tank [26,27] with a size of $1200 \times 800 \times 730$ mm, as shown in Figure 15a. The model allows for the installation of up to five electromagnetic antennas to record the PD-emitted signals: one on the sidewall, two in the oil drain, and two on the top cover, as shown in Figure 15b.

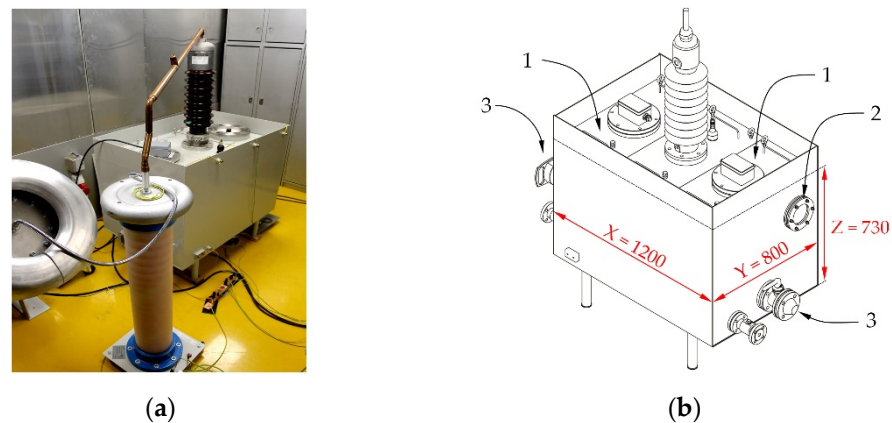


Figure 15. Realistic transformer tank. (a) Test setup arranged in the high-voltage laboratory; (b) schematic diagram of the transformer tank: 1—inspection hatch with UHF sensors (or plain cover); 2—inspection hatch with the dielectric window made of poly (methyl methacrylate) (PMMA); 3—oil drain valve [27].

Since the PD in the laboratory tests was produced by the electrode system installed in the center of the tank, the PD source modeled in CST-MWS was also located in this position. A Gaussian signal with a bandwidth of 3 GHz was used to excite the PD in this location. The PD signal was injected through a discrete port in CST-MWS in the forward phase.

Due to the requirement of high memory resources for the backward phase to record the electric field inside the tank, the monitoring region was restricted to a 40-cm^3 cubic region around the electrode system.

Figure 16 shows the distribution of the normalized maximum electric field power over the whole time interval for a square with a length of 40 cm around the electrode system obtained by the EMIF method. In this figure, the red crosses (\times) show the estimated locations of the PD source obtained by the maximum field power criterion. It can be seen that the localization error is near zero (5 mm). The actual PD location is considered in the center of the gap used to excite the electrode system. To excite the electrode system shown in Figure 17, a discrete edge port is used in the CST-MWS model. It should be noted that the same results have been obtained for the EMTR method. Therefore, the EMTR results have not been presented here.

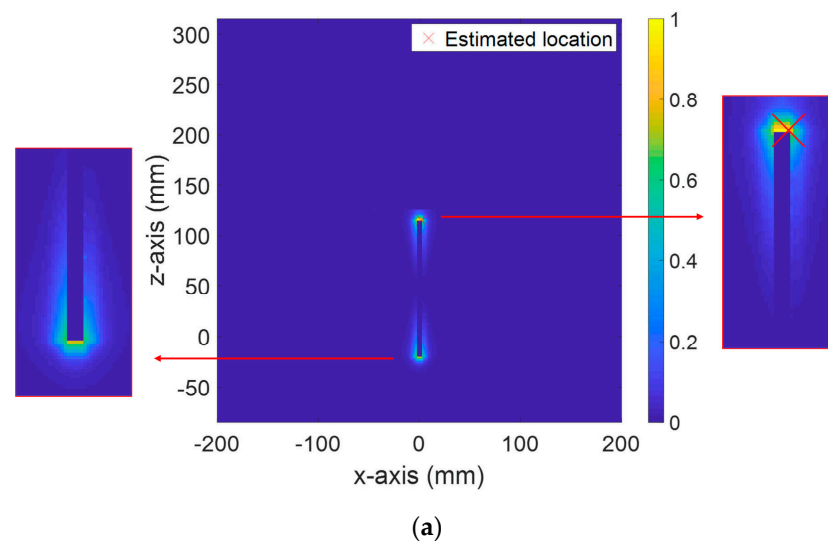


Figure 16. Cont.

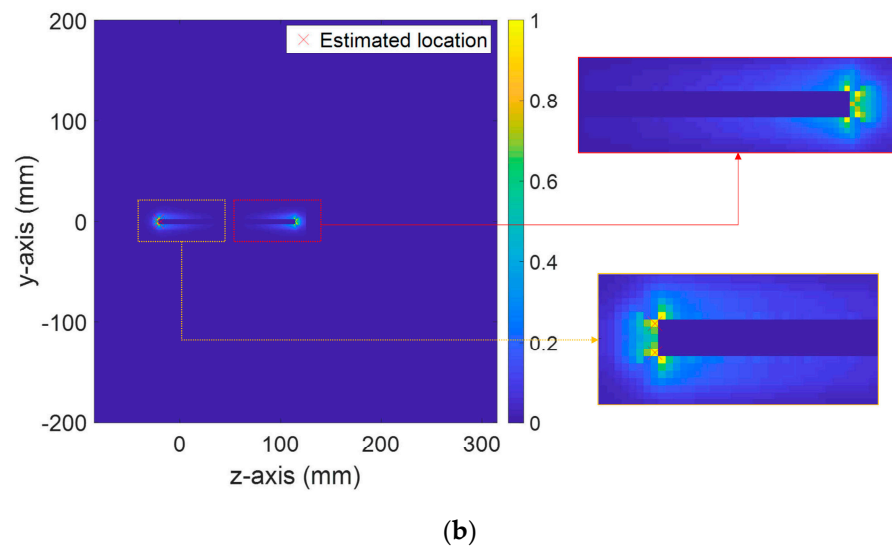


Figure 16. The distribution of normalized maximum electric field power over the complete simulation time interval in a square with a length of 40 cm around the electrode system. (a) Cut-plane xz ; (b) cut-plane yz .

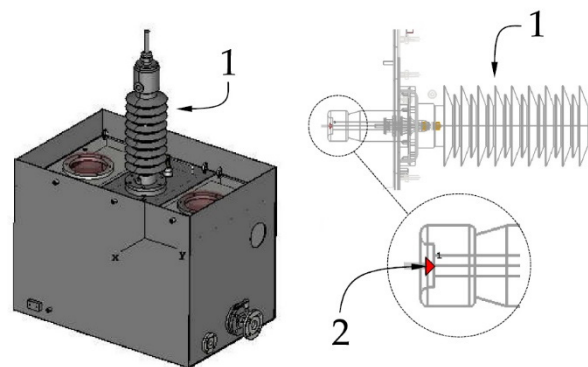


Figure 17. Realistic transformer tank 3D model used in CST-MWS: 1—110 kV transformer bushing; 2—discrete port used in CST-MWS to model the PD source located at the lower terminal of the bushing.

4. Conclusions

In this paper, a single-sensor EMIF (inverse filter method in the electromagnetic regime) method to localize PD sources in power transformers is proposed. Numerous 2D and 3D simulations have been presented to assess the performance of the proposed method. The simulation results show that the presented method is able to localize PDs with suitable accuracy using only one single sensor.

The presented simulation results also suggest that, for the conditions used in this study, the EMIF method shows better performance compared to the classical EMTR method in dealing with challenging problems involving PD sources close to metallic objects or between two metallic objects with a short distance between them.

In the last part of the paper, a simulation example is presented to show the performance of the EMIF method to locate PDs in a realistic power transformer tank.

One of the challenges of the application of the proposed model to real transformers is the need to accurately model the transformer. Indeed, the method's performance might be affected by any mismatch between the model and the real transformer tank. Future work will be devoted to the experimental validation of the proposed EMIF method. The EMIF method's performance is generally impacted by the spectrum of the source. For PDs, the EMIF method improves the location accuracy since the inverse signal has a wider spectrum.

When an arbitrary source produces a narrow-bandwidth signal, the inverted signal would have a lower bandwidth, resulting in a worse accuracy than conventional EMTR.

Author Contributions: Conceptualization, H.K., M.R. and F.R.; methodology, H.K.; software, H.K.; validation, H.K.; investigation, H.K. and F.A.; resources, M.R. and F.R.; writing—original draft preparation, F.A. and H.K.; writing—review and editing, M.R., F.R. and W.S. All authors have read and agreed to the published version of the manuscript.

Funding: This research received no external funding.

Institutional Review Board Statement: Not applicable.

Informed Consent Statement: Not applicable.

Data Availability Statement: The data that support the findings of this study are available upon reasonable request from the corresponding author.

Acknowledgments: This research was supported by the EPFL ENABLE program. The first author would like to acknowledge support from the Bakhtar Regional Electric Company, Arak, Iran.

Conflicts of Interest: The authors declare no conflict of interest.

References

1. Yaacob, M.M.; Alsaedi, M.A.; Rashed, J.R.; Dakhil, A.M.; Atyah, S.F. Review on partial discharge detection techniques related to high voltage power equipment using different sensors. *Photonic Sens.* **2014**, *4*, 325–337. [CrossRef]
2. Partial Discharges in Transformers. Available online: <https://e-cigre.org/publication/676-partial-discharges-in-transformers> (accessed on 15 July 2021).
3. Judd, M.D.; Yang, L.; Hunter, I.B.B. Partial discharge monitoring for power transformer using UHF sensors. Part 2: Field experience. *IEEE Electr. Insul. Mag.* **2005**, *21*, 5–13. [CrossRef]
4. Refaat, S.S.; Sayed, M.; Shams, M.A.; Mohamed, A. A Review of Partial Discharge Detection Techniques in Power Transformers. In Proceedings of the 2018 Twentieth International Middle East Power Systems Conference (MEPCON), Cairo, Egypt, 18–20 December 2018; pp. 1020–1025.
5. Li, Z.; Luo, L.; Zhou, N.; Sheng, G.; Jiang, X. A Novel Partial Discharge Localization Method in Substation Based on a Wireless UHF Sensor Array. *Sensors* **2017**, *17*, 1909. [CrossRef] [PubMed]
6. Markalous, S.M.; Tenbohlen, S.; Feser, K. Detection and location of partial discharges in power transformers using acoustic and electromagnetic signals. *IEEE Trans. Dielectr. Electr. Insul.* **2008**, *15*, 1576–1583. [CrossRef]
7. Hara, S.; Anzai, D.; Yabu, T.; Lee, K.; Derham, T.; Zemek, R. A Perturbation Analysis on the Performance of TOA and TDOA Localization in Mixed LOS/NLOS Environments. *IEEE Trans. Commun.* **2013**, *61*, 679–689. [CrossRef]
8. Do, J.-Y.; Rabinowitz, M.; Enge, P. Robustness of TOA and TDOA Positioning Under Suboptimal Weighting Conditions. *IEEE Trans. Aerosp. Electron. Syst.* **2007**, *43*, 1177–1180. [CrossRef]
9. Hou, H.; Sheng, G.; Li, S.; Jiang, X. A Novel Algorithm for Separating Multiple PD Sources in a Substation Based on Spectrum Reconstruction of UHF Signals. *IEEE Trans. Power Deliv.* **2014**, *30*, 809–817. [CrossRef]
10. Tomic, S.; Beko, M.; Dinis, R. Distributed RSS-AoA Based Localization with Unknown Transmit Powers. *IEEE Wirel. Commun. Lett.* **2016**, *5*, 392–395. [CrossRef]
11. Polak, F.; Sikorski, W.; Siodla, K. Location of partial discharges sources using sensor arrays. In Proceedings of the 2014 ICHVE International Conference on High Voltage Engineering and Application, Poznan, Poland, 8–11 September 2014; pp. 1–4. [CrossRef]
12. Robles, G.; Sánchez-Fernández, M.; Sanchez, R.A.; Rojas-Moreno, M.V.; Rajo-Iglesias, E.; Martínez-Tarifa, J.M. Antenna Parametrization for the Detection of Partial Discharges. *IEEE Trans. Instrum. Meas.* **2013**, *62*, 932–941. [CrossRef]
13. Robles, G.; Fresno, J.M.; Martínez-Tarifa, J.M. Separation of Radio-Frequency Sources and Localization of Partial Discharges in Noisy Environments. *Sensors* **2015**, *15*, 9882–9898. [CrossRef]
14. Xue, N.; Yang, J.; Shen, D.; Xu, P.; Yang, K.; Zhuo, Z.; Zhang, L.; Zhang, J. The Location of Partial Discharge Sources Inside Power Transformers Based on TDOA Database with UHF Sensors. *IEEE Access* **2019**, *7*, 146732–146744. [CrossRef]
15. Karami, H.; Azadifar, M.; Mostajabi, A.; Rubinstein, M.; Karami, H.; Gharehpetian, G.B.; Rachidi, F. Partial Discharge Localization Using Time Reversal: Application to Power Transformers. *Sensors* **2020**, *20*, 1419. [CrossRef] [PubMed]
16. Karami, H.; Azadifar, M.; Rubinstein, M.; Rachidi, F. An experimental validation of partial discharge localization using electromagnetic time reversal. *Sci. Rep.* **2021**, *11*, 220. [CrossRef] [PubMed]
17. Azadifar, M.; Karami, H.; Wang, Z.; Rubinstein, M.; Rachidi, F.; Karami, H.; Ghasemi, A.; Gharehpetian, G.B. Partial Discharge Localization Using Electromagnetic Time Reversal: A Performance Analysis. *IEEE Access* **2020**, *8*, 147507–147515. [CrossRef]
18. Karami, H.; Azadifar, M.; Mostajabi, A.; Rubinstein, M.; Rachidi, F. Localization of Electromagnetic Interference Source Using a Time Reversal Cavity: Application of the Maximum Power Criterion. In Proceedings of the IEEE International Symposium on Electromagnetic Compatibility, Signal Integrity and Power Integrity, Reno, NV, USA, 28 July–28 August 2020.

19. Montaldo, G.; Tanter, M.; Fink, M. Real time inverse filter focusing through iterative time reversal. *J. Acoust. Soc. Am.* **2003**, *115*, 435–438. [[CrossRef](#)]
20. Anderson, B.E.; Douma, J.; Ulrich, T.; Snieder, R. Improving spatio-temporal focusing and source reconstruction through deconvolution. *Wave Motion* **2015**, *52*, 151–159. [[CrossRef](#)]
21. Yu, X.; Zou, C.; Yang, L. Improved recursive inverse filtering method for blind image restoration. In Proceedings of the 6th International Conference on Signal Processing, Beijing, China, 26–30 August 2002; pp. 37–40. [[CrossRef](#)]
22. Moll, J.; Fritzen, C.P. Time-varying inverse filtering for high resolution imaging with ultrasonic guided waves. In Proceedings of the 10th European Conference on Non-Destructive Testing, Moscow, Russia, 7–11 June 2010.
23. Willardson, M.L.; Anderson, B.E.; Young, S.M.; Denison, M.H.; Patchett, B.D. Time reversal focusing of high amplitude sound in a reverberation chamber. *J. Acoust. Soc. Am.* **2018**, *143*, 696–705. [[CrossRef](#)]
24. Douma, J.; Niederleithinger, E.; Snieder, R. Locating Events Using Time Reversal and Deconvolution: Experimental Application and Analysis. *J. Nondestruct. Eval.* **2015**, *34*, 2. [[CrossRef](#)]
25. Derode, A.; Tourin, A.; De Rosny, J.; Tanter, M.; Yon, S.; Fink, M. Taking Advantage of Multiple Scattering to Communicate with Time-Reversal Antennas. *Phys. Rev. Lett.* **2003**, *90*, 014301. [[CrossRef](#)]
26. Sikorski, W. Development of Acoustic Emission Sensor Optimized for Partial Discharge Monitoring in Power Transformers. *Sensors* **2019**, *19*, 1865. [[CrossRef](#)]
27. Sikorski, W. Active Dielectric Window: A New Concept of Combined Acoustic Emission and Electromagnetic Partial Discharge Detector for Power Transformers. *Energies* **2019**, *12*, 115. [[CrossRef](#)]